Obesity alters ovarian folliculogenesis through disrupted angiogenesis from increased IL-10 production

Po-Kai Yang [1,7], Chia-Hung Chou [1,7], Chu-Chun Huang [1], Wen-Fen Wen [2], Hsin-Fu Chen [1,3], Chia-Tung Shun [4], Hong-Nerng Ho [1,5], Mei-Jou Chen [1,6,*]

ABSTRACT

Objective: Obesity has been reported to have a modulatory effect on the ovulatory functions of patients with polycystic ovary syndrome. The role of adipokines in this obesity-associated ovulatory disturbance has not been extensively explored. In this study, the relationships between obesity, adipokine production from visceral fat, and ovarian folliculogenesis were explored in a mice model of induced obesity.

Methods: Obesity was induced in female C57BL/6 mice fed *ad libitum* with high-fat feed and fructose water for 4 weeks. Follicular developments in the ovaries were assessed by histopathology in these diet-induced obese mice. Changes in adipokine expression in the peri-ovarian adipose tissues were screened with an adipokine array. The adipokine with the most significant increase over time was identified. The functions of the adipokine in angiogenic processes were evaluated in a cell model of endothelial proliferation. The *in vivo* effects of neutralizing this adipokine using specific antibodies were assessed in the same obesity model.

Results: A high-fat and fructose diet induced an accumulation of early ovarian follicles and a reduction in mature follicles and corpus lutea. The number of microvessels in the early follicles also decreased. The adipokine protein array of the peri-ovarian adipose tissues identified a progressive increase in IL-10 expression with the duration of the obesogenic diet. *In vitro* experiments in the endothelial cell model confirmed IL-10 as a disrupter of VEGF-induced angiogenesis. Administration of anti-IL-10 antibodies prevented the histopathological changes induced by the obesogenic diet and further highlighted the role of IL-10 in disrupting folliculogenesis.

Conclusions: Obesity may disrupt normal folliculogenesis through increased production of IL-10 in visceral fats. This relationship may help clarify the reported association between obesity and ovulatory dysfunction, which has been found in patients with polycystic ovary syndrome. However, the duration of this study was short, which limited conclusions on the long-term reproductive outcomes.

1. INTRODUCTION

Polycystic ovary syndrome (PCOS) is a common endocrinopathy among reproductive age women. Women with PCOS are characterized by oligomenorrhea, hyperandrogenism, and polycystic ovaries—the combinations of which comprise the various diagnostic criteria of PCOS [1—3]. Although not traditionally part of the diagnostic criteria, obesity is more prevalent in patients with PCOS and affects their phenotypic severity [4]. In addition to more severe glucose resistance, obesity is found to be independently associated with disturbed ovarian parameters, such as decreased anti-Müllerian hormone (AMH), lower antral follicle counts, and smaller ovarian volumes [5]. Functional disturbances in ovulation central to the phenotypic presentation of menstrual irregularity are worsened in individuals with obesity [6,7].

Evidence of a cause-and-effect relationship between obesity and ovulatory dysfunction has been found in both experimental and interventional studies. An obesogenic diet alone induced PCOS-like changes in murine models, whereby obese mice displayed more estrus cycle irregularities and higher levels of testosterone [8,9]. In addition, histopathology of the ovaries showed a greater number of large-size follicles, decreased number of corpus lutea, and increased number of hyperplastic theca cells—changes reminiscent of the histopathology of PCOS ovaries [8]. Similarly, in Ossabaw mini-pigs, hyperandrogenism, extended estrous cycles, and increased numbers of medium and cystic follicles were induced by obesogenic diets [10].

[1]Department of Obstetrics and Gynecology, National Taiwan University Hospital, Taipei, Taiwan [2]Department of Pathology, College of Medicine, National Taiwan University, Taipei, Taiwan [3]Graduate Institute of Medical Genomics and Proteomics, College of Medicine, National Taiwan University, Taipei, Taiwan [4]Department of Forensic Medicine and Pathology, College of Medicine, National Taiwan University, Taipei, Taiwan [5]College of Medicine, Taipei Medical University, Taipei, Taiwan [6]Livia Shang Yu Wan Chair Professor of Obstetrics and Gynecology, College of Medicine, National Taiwan University, Taipei, Taiwan

[7] These authors contributed equally to this study.

*Corresponding author. Department of Obstetrics and Gynecology, National Taiwan University Hospital, No. 8, Chung-Shan South Road, 100, Taipei, Taiwan. E-mail: mjchen04@ntu.edu.tw (M.-J. Chen).

Original Article

Abbreviations

AMH	anti-Müllerian hormone
ANGPTL2	angiopoietin-related protein 2
Anti-IL-10 mAb	anti-IL-10 monoclonal antibody
CXCL5	C-X-C motif chemokine ligand 5
HE	hematoxylin and eosin
HFF/FW	high-fat feed and fructose water
HPF	high-power field
HRP	horseradish peroxidase
HUVEC	human umbilical vein endothelial cell
IHC	immunohistochemistry
IL	interleukin
Ly6G	lymphocyte antigen 6 complex locus G6D
MCP-1	monocyte chemoattractant protein 1
PCOS	polycystic ovary syndrome
POAT	peri-ovarian adipose tissue
RBP4	retinol binding protein 4
SFRP5	secreted frizzle-related protein 5
STD	standard diet
TNFα	tumor necrosis factor alpha
VEGF	vascular endothelial growth factor

Conversely, interventional studies in humans have found weight reductions from dietary control alone normalized the ovulatory dysfunctions in women with PCOS [11,12]. These studies highlighted the impact of obesity on ovulatory functions.

In previous studies on obesity, the visceral fat has been identified as a mediator for many of the derangements associated with obesity, including altered glucose homeostasis, steroid production, and reproduction [13]. The role of the visceral fats in mediating ovulatory dysfunction in obesity has not been extensively explored, although visceral fat dysfunctions have long been suspected in women with PCOS. Women with PCOS were reported to be predisposed to central obesity [14]. Increased adipocyte sizes with increased production of the adipokines leptin, adiponectin, and visfatin were seen in women with PCOS [15]. These adipokines have been implicated in steroidogenic pathways [15] and were hypothetically linked to menstrual disturbances. However, the effects of abnormal adipokine production on follicular developments in the ovaries have not been systemically evaluated.

In this study, the relationships between obesity, adipokine production in the visceral fat, and folliculogenesis were assessed in a mouse model of obesity. Obesity was induced in female C57BL/6 mice using an obesogenic diet consisting of high-fat feed and fructose water (HFF/FW). Functional changes in their ovaries were evaluated with histopathology and immunohistochemistry (IHC). In addition, the peri-ovarian adipose tissues (POATs), which are considered analogous to the visceral fats of humans, were screened for changes in adipokine expression. The findings of this study may help clarify the clinical association seen between obesity and ovulatory dysfunction, which has been reported in patients with PCOS. They may also provide potential targets for future therapies.

2. MATERIALS AND METHODS

2.1. Animals

Female C57BL/6 mice were obtained from the laboratory animal center of the National Taiwan University Medical School at 5 weeks of age. The animals were housed in polysulfone cages on wood-chip bedding and provided with water and a regular commercial diet (Rodent Diet 20 #5053, PicoLab, St. Louis, MO, USA). The animals were acclimated to their surroundings for 1 week before initiating dietary manipulation. The mice quarters were air conditioned (25 °C), controlled for humidity (40−60%), and had a 12-h light/dark cycle. All the experimental protocols were approved and supervised by the Institutional Animal Care and Use Committee (IACUC) of the College of Medicine at National Taiwan University. All the animal experiments described in the submitted manuscript were conducted in accordance with the accepted standards of humane animal care.

2.2. Grouping and study protocol

2.2.1. Effects of HFF/FW diet on follicular development and AMH
The effects of the HFF/FW diet on the ovaries were evaluated using histopathology. The animals were randomly assigned at 6 weeks of age into 2 weight-matched groups and received 2 different dietary regimens: a standard diet (STD; N = 10) or HFF/FW diet (N = 10). The STD consisted of regular feed (D12450B, rodent diet 10 kcal% fat, Research Diets, New Brunswick, NJ, USA) and drinking water, while the HFF/FW diet consisted of a high-fat feed (D12492, rodent diet 60 kcal% fat, Research Diets, New Brunswick, NJ, USA) and 20% fructose (Sigma-Aldrich) water by volume. Both diets were given *ad libitum* for 4 weeks. The mice were weighed weekly from the start of the study and sacrificed under anesthesia with 5% isoflurane (Sigma-Aldrich) at the end of the 4-week study period. Blood was collected via cardiac puncture and the ovaries were dissected, fixed in 4% formaldehyde, and embedded in paraffin. All animals in the same treatment group were housed together, and soiled beddings from a male mouse were introduced 1 week before sacrifice to synchronize the estrus cycles via the Lee-Boot [16] and Whitten effects [17].

2.2.2. Effects of HFF/FW duration on adipokine expression in the POATs and serum
The effects of different durations of the HFF/FW diet on adipokine expression in the POATs were evaluated. The animals were again allocated into STD (N = 40) and HFF/FW (N = 40) diets at 6 weeks of age. After each completed week of dietary manipulation over a 4-week period, mice (N = 10/group/week) were randomly chosen from each treatment group and sacrificed under anesthesia with 5% isoflurane. Blood and ovaries were collected using the methods described in Section 2.2.1. The POATs were harvested and stored in liquid nitrogen for subsequent protein extraction and assay.

2.2.3. Effects of anti-murine anti-IL-10 monoclonal antibody (anti-IL-10 mAb) on HFF/FW-induced changes in follicular development
The effects of anti-IL-10 mAb on changes in folliculogenesis induced by the HFF/FW diet were evaluated. The HFF/FW models were established using the same methods as in Section 2.2.1. Briefly, animals were obtained at 5 weeks of age, and the HFF/FW diet was initiated at 6 weeks. At initiation of the HFF/FW diet, the animals were randomly assigned into 2 weight-matched groups. The control group (N = 10) received isotype IgG (R&D Systems), while the experimental group (N = 10) received anti-IL-10 mAb (R&D Systems). The antibodies were given twice weekly by intraperitoneal injection (100 μg/mouse), and both groups were fed HFF/FW diets for 4 weeks. The same experiment was performed in the STD mice, wherein one group received isotype IgG (N = 10) and the other received anti-IL-10 mAb (N = 10) for 4 weeks. At the end of the 4-week period, the animals were sacrificed under anesthesia with 5% isoflurane, and the blood, ovaries, and POATs were collected as described in Section 2.2.2.

2.3. Ovarian histopathology and classification of follicle development and counts

The ovaries were serially sectioned in the long axis at 5-µm intervals and every fifth section was stained with hematoxylin and eosin (HE). The section with the largest diameter of each ovary was chosen as the representative section for that ovary. For each representative section, counts of the total number of follicles and number of follicles at each developmental stage were determined. All the follicles with intact, non-fragmented oocytes on the representative sections were counted and classified by developmental stage. The developmental stage for a particular follicle was determined after reviewing all the adjacent sections containing the follicle. All the histopathology counts and classifications of the follicles were performed by two observers who reviewed the slides in collaboration before finalizing the counts. Both observers were blinded to the treatment group. One ovary from each mouse (N = 10/group) was examined, and the counts from each representative section were averaged over the treatment group.

The developmental stages of the follicle were classified according to published reports [18,19]. A primary follicle was defined as an oocyte encircled by one single layer of cuboid granulosa cells, a secondary follicle was characterized by two or more layers of granulosa cells without a visible antrum, and a tertiary follicle was identified by the presence of an antrum. Tertiary follicles were further divided into early and late tertiary follicles based on the projected oocyte maturity. Pre-ovulatory (Graafian) follicles and follicles with diameters $\geq$ 250 µm, a criterion reported to be a good indicator of oocyte maturity in mice [20], were categorized as late tertiary follicles. Tertiary follicles without these developmental features were categorized as early tertiary follicles. Corpus lutea were characterized by theca-lutein and granulosa-lutein cells. The primary and secondary follicles were counted at 400x magnifications, and the tertiary follicles and corpus luteum were counted at 40x magnifications.

2.4. Immunohistochemistry

The ovarian sections were deparaffinized, rehydrated in phosphate-buffered saline (PBS) for 15 min, and the endogenous peroxidases were inhibited with 3% H_2O_2/methanol for 10 min at room temperature. These were followed by microwaving in 0.01 M of citrate buffer (pH 6.0) for antigen retrieval. The slides were then blocked with 5% non-fat milk/PBS for 30 min at room temperature and incubated for 16 h at 4 °C with specific antibodies for Ki67 (sc-23900; 1:200 dilution), CD34 (sc-74499; 1:200 dilution), and IL-10 (sc-365858; 1:100 dilution) from Santa Cruz Biotechnology (Santa Cruz, CA, USA). The peroxidase-conjugated secondary antibody was added for 1 h at room temperature, and the slides were developed by immersing in 0.06% 3,3′-diaminobenzidine (DAKO) and counterstaining with Gill's Hematoxylin V. For double-stained IHC, the slides were first stained with IL-10 as previously described (brown) and processed for immune cells using CD45R (sc-19615; 1:50 dilution), Ly6G (sc-53515; 1:50 dilution), or F4/80 (sc-377009; 1:50 dilution). The secondary antibodies were followed by a Vulcan Fast Red kit to produce a bright fuchsin-red precipitate, and the slides were counterstained with Gill's Hematoxylin V.

2.4.1. Granulosa cell proliferation

The percentage of Ki67-positive granulosa cells in a follicle was calculated as the number of Ki67-stained granulosa cells divided by the total number of granulosa cells counted under 400x magnification. One early tertiary follicle per representative section was randomly chosen at 40x magnification for quantification. The total numbers of granulosa cells and number of Ki67-positive granulosa cells in the early tertiary follicle were counted, and a positive staining percentage was calculated. The calculated percentages were averaged over all the follicles in the treatment group (N = 10/group).

2.4.2. Microvessel count

A microvessel count was performed according to our previous protocol [21]. Briefly, after immunostaining with CD34 antibody to localize endothelial cells, microvessels in the early tertiary follicles were quantified using light microscopy. A representative section from each ovary was examined at a low magnification (40x) to randomly identify an early tertiary follicle. The number of microvessels within the examined early tertiary follicle was determined under a high magnification (400x) by counting the number of independent clusters of CD34-positive cells, which represented endothelial cells. The number of counted microvessels was averaged over all the follicles in the treatment group (N = 10/group).

2.5. POAT lysates

The POATs from one ovary from each mice were homogenized and extracted for proteins in lysis buffer. The proteins from the tissue lysates were quantified using a Bio-Rad protein assay (Bio-Rad Laboratories, Hercules, CA, USA). Equal quantities of the POAT lysates from each mouse (200 µg/mouse) were pooled by diet group and treatment durations (N = 10/group/week). These were submitted for adipokine arrays.

2.6. POAT cultures and conditioned medium

The secretion of IL-10 by the POATs was quantified in cell cultures in accordance with a published methodology [22]. The POATs were weighed, cut into small pieces, and incubated in Dulbecco's Modified Eagle's Medium (DMEM; Thermo Fisher Scientific, 11995065) containing 10% FBS for 24 h at 37 °C. The medium was collected for IL-10 quantification using an ELISA kit (R&D Systems). The detected IL-10 levels were normalized by POAT weight.

2.7. Adipokine array

A mouse adipokine array (Proteome Profiler, R&D Systems) was used to analyze the adipokine protein profiles from the pooled POAT lysates (see Section 2.5). The pooled POAT lysates were first mixed with a biotinylated detection antibody cocktail at room temperature for 1 h, while the array membranes were blocked with blocking solution. The membranes were then incubated with the samples overnight on a shaker at 2–8 °C. After washing, horseradish peroxidase-conjugated streptavidin was added to the membranes at room temperature for 30 min, and signals were developed with commercial chemiluminescent detection reagents. A digital imaging system (Bio Pioneer Tech Co., New Taipei City, Taiwan) was used to capture the signals, and further analyses were performed using ImageJ [23].

2.8. IL-10 and AMH quantification

Changes in IL-10 expression in the POATs were confirmed using ELISA on prepared tissue lysates of individual POATs (see Section 2.5). The POAT lysate and serum (N = 10/group/week) from each mouse were quantified for IL-10 using a Mouse IL-10 Quantikine ELISA kit (R&D Systems). AMH levels were determined from the mice serum using a Mouse AMH ELISA kit (Cusabio Biotech Co., Houston, TX, USA).

2.9. Human umbilical vein endothelial cell (HUVEC) cultures

HUVECs were purchased from the American Type Culture Collection (Rockville, MD, USA) and cultured at 37 °C with 5% CO_2 in endothelial cell growth medium (Cell Applications Inc., San Diego, CA, USA). Prior

to experimentations, the HUVECs were washed with PBS twice to remove residuals and all the experiments were performed between the third and fifth passages.

2.9.1. Tube formation assay

The effects of IL-10 on the formation of capillary-like structures induced by vascular endothelial growth factor (VEGF) were investigated in the HUVECs grown on Matrigel per published protocols [24]. Cells were seeded at 1×10^3 cells/well on 96-well plates in wells coated with Cultrex Basement Membrane Extract (BME, R&D Systems). These were then cultured in serum-free M199 medium in the presence of vehicle (control), VEGF (50 ng/ml; recombinant human VEGF; R&D Systems) alone, VEGF (50 ng/ml) plus low-dose IL-10 (10 pg/ml; recombinant human IL-10; R&D Systems), VEGF (50 ng/ml) plus high-dose IL-10 (100 pg/ml), or high-dose IL-10 (100 pg/ml) alone. After incubation for 5 h, the total number of capillaries and tube-like structures (complete loop structures) per well in each treatment group were counted, and representative photos of the capillary-like structures were taken.

2.9.2. Cell migration assay

The effects of IL-10 on endothelial cell migration were assessed. The HUVECs were cultured on 24-well plates and grown to confluence. A scratch was made at the center of each well using the tip of a 1 ml plastic pipette to denude a section of the culture wells. The adherent cells were washed twice with PBS and then incubated in M199 with 2% BSA (bovine serum albumin; Sigma-Aldrich), mitomycin C (150 μM; Sigma-Aldrich) and vehicle (control), VEGF (50 ng/ml) alone, VEGF (50 ng/ml) plus low-dose IL-10 (10 pg/ml), VEGF (50 ng/ml) plus high-dose IL-10 (100 pg/ml), or high-dose IL-10 (100 pg/ml) alone. After 16 h of incubation, the cells were washed twice with PBS, fixed with 2% formalin, stained with 1% crystal violet, and photographed. The migrations of the HUVECs were quantified as the areas covered by the migrating HUVECs relative to the initial denuded areas.

2.9.3. Endothelial monolayer permeability

The HUVECs were seeded on Transwell chambers with 0.4 μm pore-sized polycarbonate membranes (Costar, Cambridge, MA, USA) and grown to confluency to form a monolayer. The HUVECs were pretreated with medium alone (control), VEGF (50 ng/ml) alone, VEGF (50 ng/ml) plus low-dose IL-10 (10 pg/ml), VEGF (50 ng/ml) plus high-dose IL-10 (100 pg/ml), or high-dose IL-10 (100 pg/ml) alone. Horseradish peroxidase (HRP; Sigma-Aldrich) at a concentration of 0.1 μM was added to the upper chamber. HRP diffusion through the HUVEC monolayer was measured and used to represent permeability. After incubation for 1 h, the medium in the lower chamber was assayed for HRP activity using a photometric guaiacol substrate assay (Sigma-Aldrich). The permeability was calculated by dividing the HRP concentration in the lower chamber medium by the initial HRP concentration in the upper chamber. The results from all the wells were normalized by the control wells and shown as percentages.

2.9.4. Cell proliferation assay

Cell proliferation was determined by MTT assay (Thermo Fisher Scientific). Briefly, the HUVECs were plated onto 96-well plates at a concentration of 1×10^3 cells/well and incubated for 72 h with vehicle (control), VEGF (50 ng/ml) alone, VEGF (50 ng/ml) plus low-dose IL-10 (10 pg/ml), VEGF (50 ng/ml) plus high-dose IL-10 (100 pg/ml), or high-dose IL-10 (100 pg/ml) alone. Then 20 μL of the MTT stock solution was added to each well and incubated for 4 h in the dark for reduction. DMSO (50 μL) was added to each well and thoroughly mixed with a pipette. The absorbance was read at 570 nm using an automated spectrophotometer. The results were normalized by the control wells and shown as percentages.

2.9.5. Active caspase-3 assay

Apoptotic activities in response to treatment with the various combinations of VEGF and IL-10 in the HUVECs were assessed using an active caspase-3 assay. HUVECs were cultured in 6-well plates (5×10^4 cells/well) and incubated overnight. After treatments with vehicle (control), VEGF (50 ng/ml) alone, VEGF (50 ng/ml) plus low-dose IL-10 (10 pg/ml), VEGF (50 ng/ml) plus high-dose IL-10 (100 pg/ml), high-dose IL-10 (100 pg/ml) alone, or staurosporine (positive control), cytosolic proteins of the HUVECs were isolated using Abcam's Cell Fractionation kit (Standard Cell Fractionation kit; ab109719). The concentrations of cytosolic proteins were quantified using a Bio-Rad protein assay reagent (Bio-Rad Laboratories, Hercules, CA, USA). Quantification of active caspase-3 was performed on the cytosolic proteins using a Human Active Caspase-3 Quantikine ELISA kit (R&D Systems).

2.9.6. Western blotting analyses

After treatment with the different combinations of VEGF and IL-10, the HUVECs were submitted for Western blotting to determine the expression of p-AKT/AKT. The HUVECs were lysed using a lysis buffer (Thermo Fisher Scientific) and centrifuged at 12,000 rpm for 25 min at 4 °C. The cell lysates were quantified using a Bio-Rad protein assay (Bio-Rad Laboratories, Hercules, CA, USA). A total of 50 μg of protein per sample was collected using SDS-PAGE, transferred onto polyvinylidene difluoride (PVDF) membranes, and immune-blotted with antibodies for p-AKT and AKT, respectively. Antibody bindings were detected using the appropriate peroxidase-coupled secondary antibodies and an enhanced chemiluminescence detection system (ECL, Boehringer Mannheim, Indianapolis, IN, USA). Photographs were obtained using a digital imaging system (Bio Pioneer Tech Co., New Taipei City, Taiwan).

2.9.7. Luciferase reporter assay

Determination of NF-κB promoter activities in the HUVECs treated with the different combinations of VEGF and IL-10 was performed using a luciferase reporter assay. The HUVECs (1×10^7 cells) were transfected with NF-κB-binding site-driven luciferase vector (BD Biosciences) using Transfast Transfection Reagent (Promega, Madison, WI, USA) according to the manufacturer's instructions. After transfection, the HUVEC cells were incubated in culture medium for 24 h, after which they were stimulated for 4 h with vehicle (control), VEGF (50 ng/ml) alone, VEGF (50 ng/ml) plus low-dose IL-10 (10 pg/ml), VEGF (50 ng/ml) plus high-dose IL-10 (100 pg/ml), or VEGF (50 ng/ml) plus a NF-κB inhibitor (BAY117082; 100 nM) as a positive control. The relative fold increase in luciferase activity was calculated to determine NF-κB activities.

2.9.8. Immunofluorescence staining of the NF-κB p65 subunit

The HUVECs (1×10^6 cells/ml) were seeded on cover slips. After the experimental conditions involving different combinations of VEGF and IL-10 were applied, the cells were fixed with 2% paraformaldehyde, permeabilized with 0.1% Triton X-100, incubated with anti-p65 Ab (sc-8008, 1:100 dilution; Santa Cruz Biotechnology, Santa Cruz, CA, USA), and exposed to FITC-conjugated secondary antibody (1:200 dilution; Santa Cruz Biotechnology). The integrity of the nuclei was confirmed with DAPI (1:1000 dilution; Sigma-Aldrich) staining. The locations of the NF-κB p65 subunit and nucleus were visualized under a fluorescence microscope (Nikon, Tokyo, Japan) and photographed using a digital imaging system (Bio Pioneer Tech Co., New Taipei City, Taiwan).
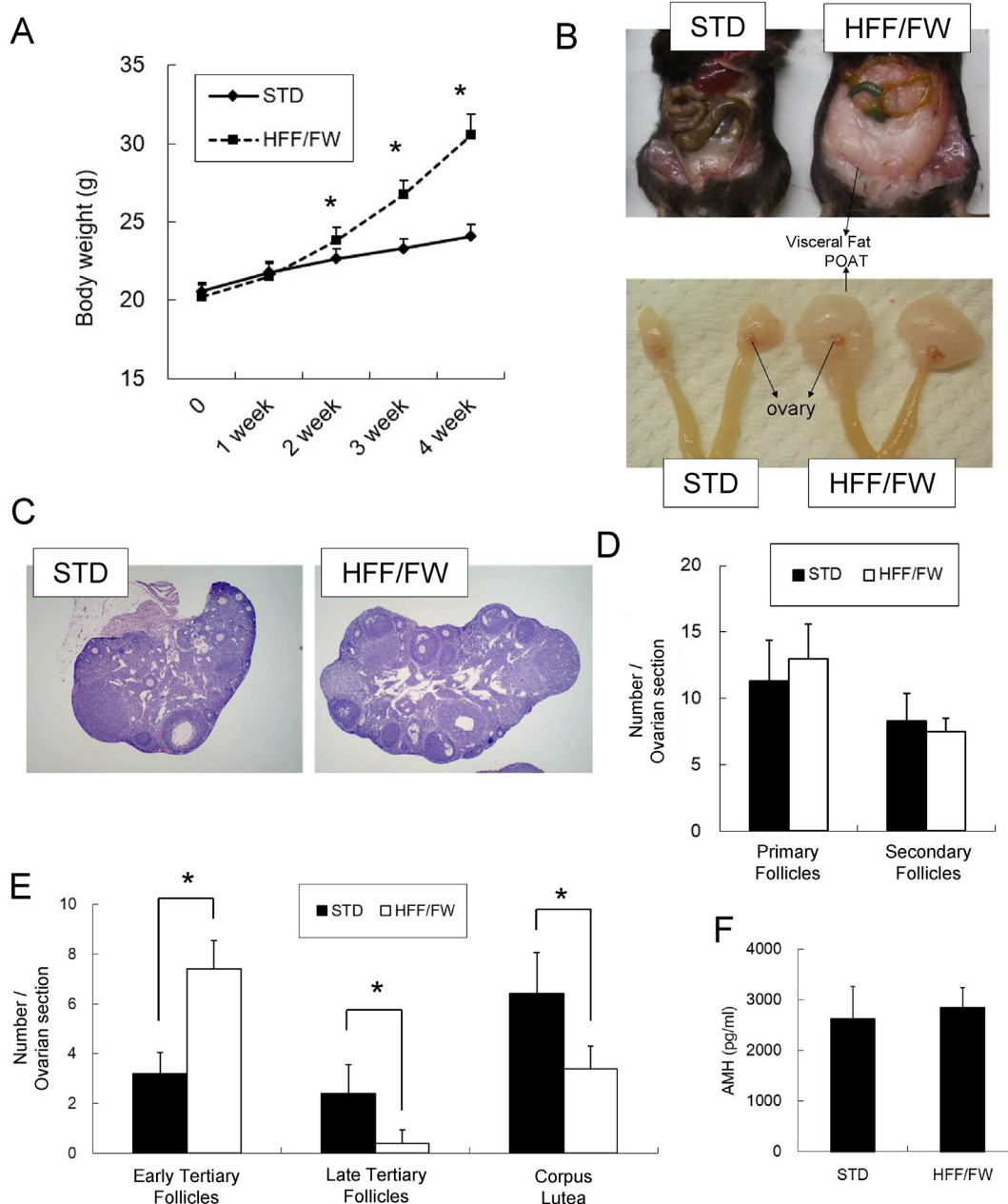
Figure 1: Effects of HFF/FW diet on weight gain, abdominal adipose, POATs, and ovarian functions. Female C57BL/6 mice were assigned to STD or HFF/FW diets for 4 weeks. (A) Changes in body weights over the 4 weeks are shown (N = 10/group). Anatomical and histological changes associated with STD and HFF/FW diets are shown in (B to F). After 4 weeks, hypertrophy of the abdominal fat pads (B: upper panel) and POATs (B: lower panel) in relation to the uteruses and ovaries were seen. Histological changes in the ovaries (40x) are shown in (C). Quantified differences in primary and secondary follicle counts (D), early, late tertiary (Graafian) follicles, and corpus luteum counts (E) are shown. Levels of AMH in the STD and HFF/FW mice are shown (F). Quantified results are expressed as mean ± SD; (*) marks statistically significant differences between groups ($P < 0.05$).

2.10. Statistical analysis

All the experiments on the endothelial cell model for angiogenic activities were repeated at least three times. Numerical data are expressed as the mean ± standard deviation. The Mann-Whitney U test was used for between-group comparisons. One-way analysis of variance (ANOVA) with Duncan's post hoc test was performed for multiple-group comparisons. P values less than 0.05 were considered statistically significant. All statistical analyses were carried out using the Statistical Analysis System (SAS version 9.3; SAS Institute Inc., Cary, NC, USA).

3. RESULTS

3.1. HFF/FW diet increased visceral fats and POATs and affected ovarian antral follicle maturation

Female C57BL/6 mice were fed the HFF/FW diet for 4 weeks to induce obesity in the HFF/FW group. After the second week, significant increases in body weight over the STD mice were seen in the HFF/FW mice (Figure 1A). Significant hypertrophy of the abdominal adipose and POATs was seen in the HFF/FW mice at 4 weeks (Figure 1B). To
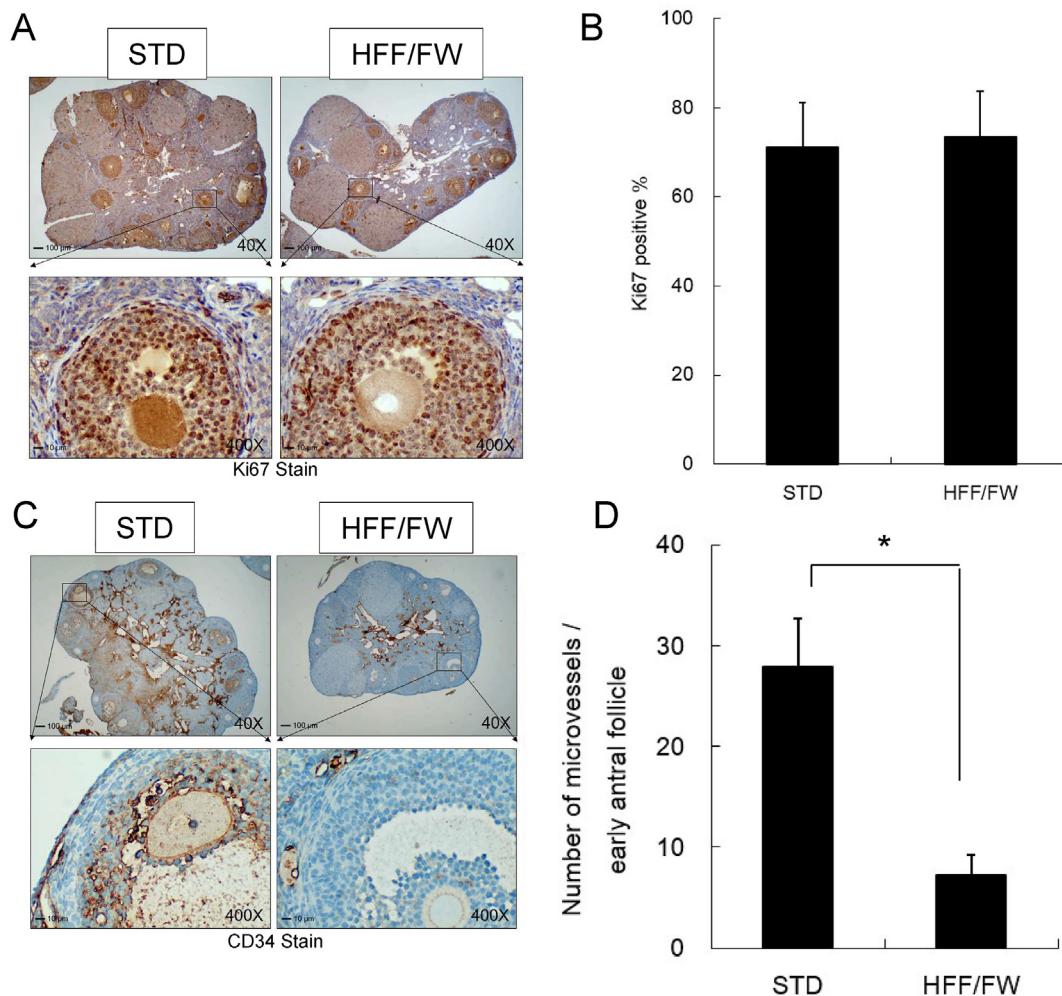
Figure 2: IHC for granulosa cell proliferation and microvessel counts in the early tertiary follicles. Differences in ovarian histology after 4 weeks of the STD and HFF/FW diets were further evaluated in the early tertiary follicles using IHC. (A) IHC with the cell proliferation marker Ki67 on low (40x) and high magnifications (400x) showed no changes in granulosa cell proliferation. (B) The percentages of cells with positive nuclear Ki67 stains in the early tertiary follicles are shown. (C) IHC with the endothelial marker CD34 on low (40x) and high magnifications (400x) showed fewer positive-stained cells in the early tertiary follicles of the HFF/FW mice. (D) The number of microvessels per early tertiary follicle was lower in the HFF/FW mice. Quantified results are expressed as mean $\pm$ SD; (*) marks statistically significant differences between groups ($P < 0.05$); N = 10/group.

determine the effects of obesity on follicle development in the ovaries, histopathological evaluations of the ovaries were performed in the HFF/FW and STD mice (Figure 1C–F). The number of primary and secondary follicles was not different between the 2 groups (Figure 1D). The number of early tertiary follicles increased, while the number of late tertiary follicles and corpus lutea decreased in the HFF/FW mice (Figure 1E). The serum levels of AMH at the end of the 4-week treatment were not different between the 2 groups (Figure 1F).

3.2. The HFF/FW suppressed angiogenesis of early antral follicles but not the proliferative activity of ovarian granulosa cells
Development of ovarian follicles usually progresses from early tertiary follicles to late tertiary follicles, after which a corpus luteum forms after ovulation. There appeared to be a developmental block between the stages of early and late tertiary follicles in the HFF/FW mice, whereby increased an number of early tertiary follicles was seen, while the number of late tertiary follicles and corpus lutea decreased. To investigate the cause of this change, IHC was performed with Ki67, a cell proliferation marker, and CD34, an endothelial marker. As shown

in Figure 2, the expression of Ki67 in the granulosa cells of the early tertiary follicles was not different between the STD and HFF/FW mice (Figure 2A,B). In contrast, microvessel counts assessed by CD34 were significantly lower in the early tertiary follicles of the HFF/FW mice compared with the STD mice (Figure 2C,D).

3.3. Expression of IL-10 increased in the POATs and serum of the HFF/FW mice
The POATs from the HFF/FW and STD groups were dissected after different durations (weeks) of dietary manipulation (N = 10/group/week). Adipokine expression was assessed in the POAT lysates using a mouse adipokine protein array. The adipokine array employed in this study had a panel of 38 adipokine proteins. Photographs of the developed slides from the adipokine arrays and final quantified results are shown in the supplement (Supplementary Figure 1 and Supplementary Table 1). The results of the adipokine array showed a progressive increase in IL-10 from the third to fourth weeks in the HFF/FW group (Figure 3A). IL-10 expressions in the mouse serum and POATs were examined with ELISA to confirm the
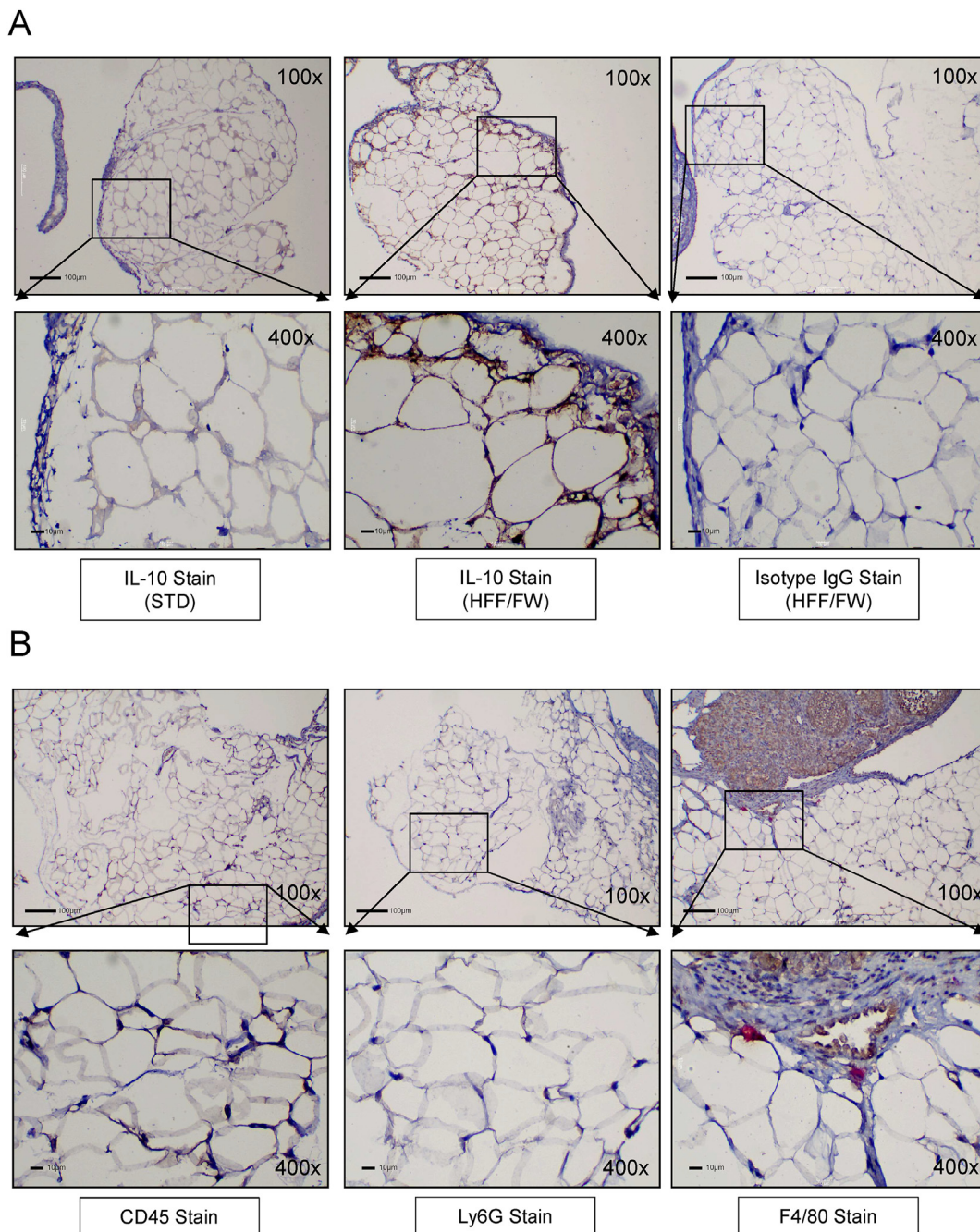
Figure 3: Concentrations of IL-10 in the POAT lysates, serum, and conditioned medium of POAT cultures. Adipokine concentrations of the pooled POAT lysates (N = 10/week) were assessed using an adipokine array after each week of the HFF/FW diet in (A). The bar chart summarizes the fold changes from the second to fourth weeks in relation to the first week for each adipokine. Changes in IL-10 (pg/ml) in the mice serum (B) and POAT lysates (C) were compared between the STD and HFF/FW groups using an ELISA kit; N = 10/week/group. (D) Conditioned medium from the POAT cultures of the HFF/FW mice had higher concentrations of IL-10; N = 5/group. Quantified results are expressed as mean ± SD; (#) marks statistically significant differences from the first week's values of the same group (P < 0.05); (*) marks statistically significant differences between groups (P < 0.05).

results of the adipokine array (Figure 3B,C). A progressive increase in IL-10 with the duration of the HFF/FW diet was seen in the serum, but pair-wise comparisons to week 1 values were significant only after the third week (Figure 3B). In contrast, the increased expression of IL-10 in the POATs was significantly different from week 1 values and also from the STD group after 2 weeks (Figure 3C). Conditioned medium from cultured POATs of the HFF/FW mice

showed significantly higher IL-10 secretion compared with the POATs of the STD mice (Figure 3D).

3.4. IHC for IL-10 and leukocyte markers in the POATs of the HFF/FW and STD mice

IHC for IL-10 in the POATs showed strong stains for IL-10 in the areas surrounding the adipocytes of the HFF/FW mice (Figure 4A, middle

A

B

Figure 4: IHC for IL-10 and leukocyte markers in the POATs of the HFF/FW and STD mice. IHC for IL-10 alone and in combination with the leukocyte markers in the POATs after 4 weeks of the STD and HFF/FW diets are shown. (A) IHC for IL-10 (brown) showed strong positivity of tissue around the adipocytes in the HFF/FW mice, but weak IL-10 staining in the STD mice. IHC for isotype IgG in the HFF/FW mice are provided for reference. (B) Common leukocyte marker CD45, myeloid marker Ly6G, and macrophage marker F4/80 (red) showed insignificant infiltration of leukocytes in the POAT. A small number of macrophages were identified, but double-stained IHC for IL-10 (brown) showed no overlaps with the leukocyte markers. Representative sections are shown at 100x and 400x magnifications.

panel). This was in contrast to the weak staining of IL-10 in the POATs of the STD mice (Figure 4A, left panel) and the negative staining of isotype IgG in the POATs of the HFF/FW mice (Figure 4A, right panel). Double staining of the POATs with IL-10 (brown) and common leukocyte marker CD45, myeloid marker Ly6G, or macrophage marker F4/80 (red) showed insignificant leukocyte infiltration and few macrophages (Figure 4B). There were no overlaps between the stains for IL-10 and the macrophage marker F4/80.

3.5. IL-10 inhibited VEGF-induced angiogenetic functions in endothelial cells *in vitro*

To test whether IL-10 was functionally responsible for the histopathological changes seen in the ovaries of the HFF/FW mice, experiments were performed on the endothelial cell model. Using the HUVEC angiogenesis model, we investigated whether the addition of IL-10 affected VEGF-induced endothelial cell survival, proliferation, migration, vascular permeability, and tube formation *in vitro* (Figure 5A—E).
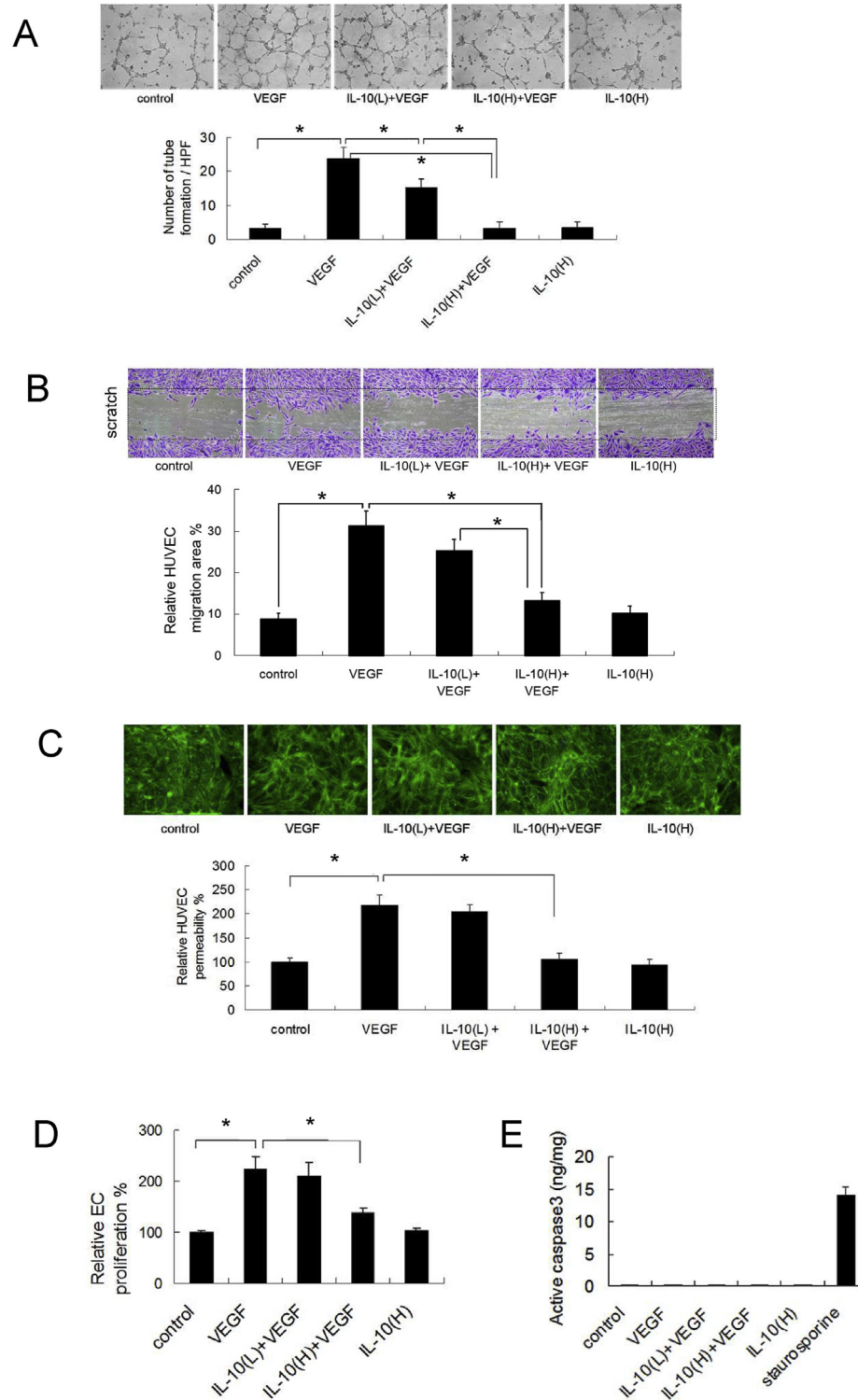
Figure 5: IL-10 inhibited angiogenic functions of HUVECs *in vitro*. Endothelial cell assays were performed using VEGF-stimulated (50 ng/ml) HUVECs. The addition of low (L) and high (H) doses of IL-10 on multiple angiogenic functions was evaluated. (A) Tube formation assay: Decreased number of tube-like structures were seen with the increased concentration of IL-10 (upper panel), while quantified results showed significant decreases associated with the addition of IL-10 (lower panel). (B) Cell migration assay: Decreased HUVECs migrations were seen in the presence of IL-10 (upper panel), while quantification by migration area showed significant differences (lower panel). (C) Gap-formation assay: formations of gaps in the HUVECs induced by VEGF were visualized using phalloidin staining. The addition of IL-10 decreased the sizes of the gaps (upper panel) as confirmed by the decreased permeability of the HUVEC monolayer to horseradish peroxidase (lower panel). (D) MTT assay: HUVECs demonstrated increased proliferation with VEGF, while the addition of IL-10 inhibited VEGF-induced proliferation. (E) Cell apoptosis assay: Activity of active caspase-3 was assessed in HUVEC cell lysates, which showed low cellular apoptosis at the indicated doses of VEGF and IL-10. Staurosporine (1 μM), an inducer of apoptosis, was used as a positive control. Quantified results are expressed as mean ± SD; IL-10 (L): 10 pg/ml; IL-10 (H): 100 pg/ml; (*) marks statistically significant differences between groups (P < 0.05). All the experiments were performed 3 times.
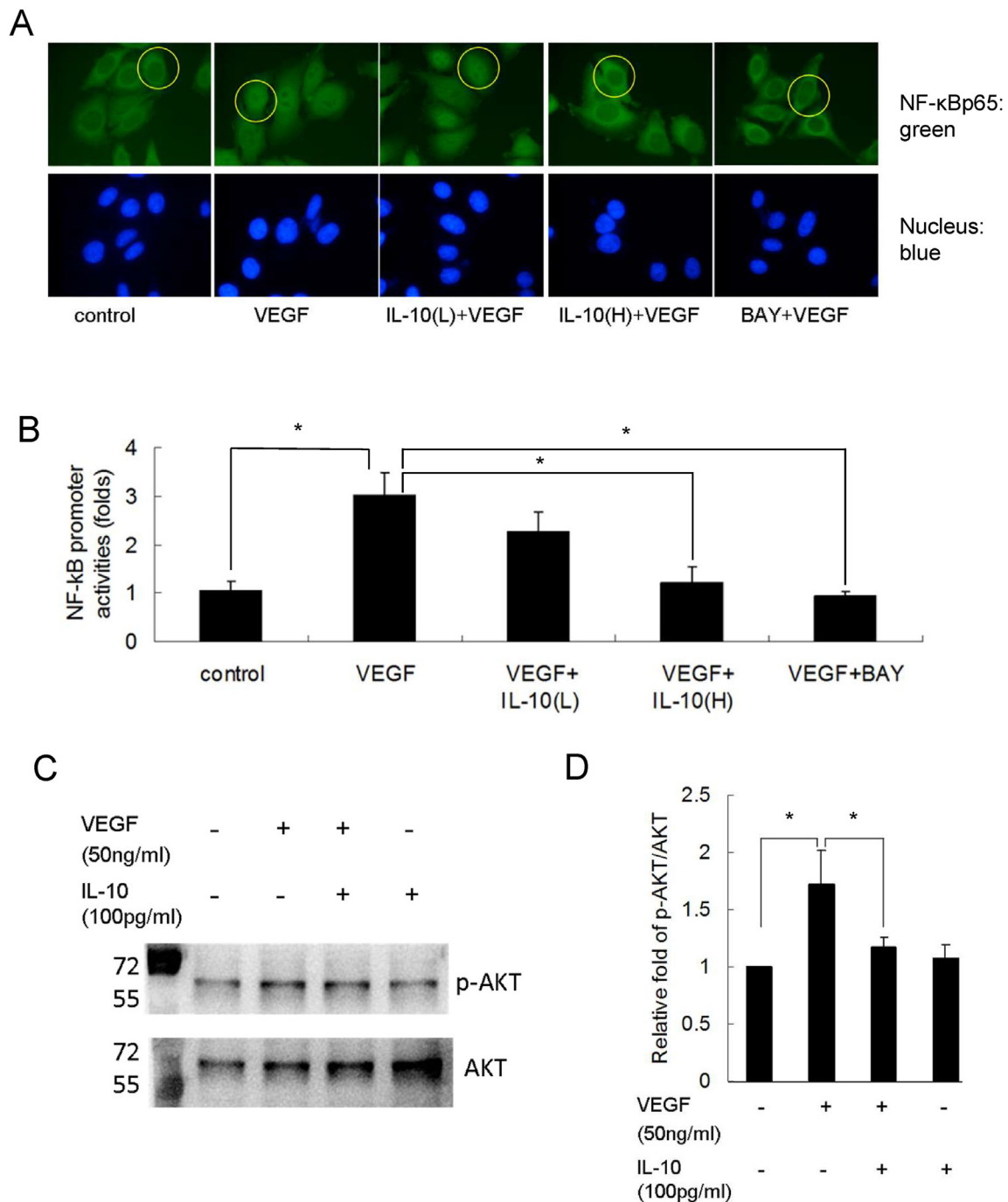
Figure 6: IL-10 inhibited NF-κB signaling and p-AKT in HUVECs *in vitro*. The molecular signaling of NF-κB and p-AKT in VEGF-stimulated (50 ng/ml) HUVECs was investigated. (A) Nuclear translocation of NF-κB p65 (immunofluorescent green) was seen in the presence of VEGF, while dose-dependent inhibitions of nuclear translocations were observed with the addition of IL-10 (upper panel). BAY117082 (BAY; 100 nM), a NF-κB chemical inhibitor, served as a positive control. The locations of the nuclei in relation to the cells are shown using blue DAPI stain for nuclei (lower panel). (B) Transfection of the HUVECs with NF-κB binding site-driven luciferase reporter plasmids showed decreased levels of NF-κB promoter activity with the addition of IL-10 and BAY117082. (C) and (D) p-AKT/AKT expression was assayed with Western blotting and quantified as fold changes over lane 1 of the control group. IL-10 significantly decreased the expression of p-AKT. ImageJ was used to determine the relative density of each lane. Quantified results are expressed as mean ± SD; IL-10 (L): 10 pg/ml; IL-10 (H): 100 pg/ml; (*) marks statistically significant differences between groups ($P < 0.05$). All the experiments were performed 3 times.

In the tube-formation assay, tube formation was evident in the HUVECs grown in VEGF-only medium. The addition of low and high doses of IL-10 significantly inhibited the VEGF-induced tube formation (Figure 5A) in a dose-dependent manner. High-dose IL-10 also significantly inhibited VEGF-induced endothelial cell migration into the denuded area on endothelial cell migration assays (Figure 5B). The vascular permeability test assessed the effects of IL-10 on gap formation and vascular permeability of the confluent HUVECs. VEGF stimulated gap formation (Figure 5C, upper panel) and increased the permeability of the HUVEC monolayer by 2 fold (Figure 5C, lower panel), while high-

dose IL-10 reduced the VEGF-induced gap formation and vascular permeability (Figure 5C). An MTT assay for cell proliferation showed VEGF stimulated the growth of the HUVECs, while the addition of high-dose IL-10 significantly reduced the proliferation (Figure 5D). Cell lysates from the various experiments were submitted for an apoptosis assay using active caspase-3 (Figure 5E). Compared with staurosporine (positive control), all the treatments with VEGF and IL-10 showed low levels of active caspase-3 (Figure 5E). This demonstrated that the effects of VEGF and IL-10 did not derive from cytotoxic effects and likely reflected cellular responses.

3.6. IL-10 suppressed VEGF-activated NF-κB signaling and p-AKT expression in endothelial cells

VEGF has been found to be a critical factor in the formation of antral follicles [25]. We therefore investigated the molecular role of IL-10 in VEGF signaling. Fluorescent staining for NF-κB p65 demonstrated VEGF to be an inducer of NF-κB nuclear translocation. The addition of high-dose IL-10 reduced the VEGF-activated nuclear translocation of NF-κB (Figure 6A), similar to treatments with the NF-κB inhibitor BAY117082 (positive control). In addition, the NF-κB promoter assay showed significant NF-κB-driven promoter activities in the presence of VEGF, while the addition of high-dose IL-10 and NF-κB inhibitor BAY117082 significantly reduced the NF-κB driven promoter activities in the HUVECs (Figure 6B). To determine the effects of IL-10 on PI3K/AKT signaling, Western blotting (Figure 6C) of the HUVEC lysates cultured in VEGF was compared with those co-cultured in VEGF and high-dose IL-10. VEGF alone increased p-AKT expression, while VEGF with high-dose IL-10 showed reduced p-AKT expression. The quantified Western blotting results are shown in Figure 6D.

3.7. Anti-IL-10 mAb mitigated the decrease in late tertiary follicle and corpus lutein counts and the decrease in microvessel numbers in the early tertiary follicles of the HFF/FW mice in vivo

The previous experiments established a role for IL-10 in the inhibition of VEGF-mediated angiogenic functions in the HUVECs. While these experiments provided evidence of IL-10 involvement in endothelial proliferation, they did not establish a direct relationship between IL-10 and folliculogenesis. Therefore, we investigated whether blocking the activities of IL-10 with neutralizing antibodies prevented the altered follicular development found in the HFF/FW mice. Treatments with anti-IL-10 mAb resulted in more prominent CD34 staining in the early tertiary follicles compared with treatment with isotype IgG (Figure 7A). The microvessel counts per early tertiary follicle in the anti-IL-10 mAb-treated HFF/FW mice were higher than in the isotype antibody-treated HFF/FW mice (Figure 7B). This effect was not seen in the STD mice treated with the same anti-IL-10 mAb (Figure 7B). A higher number of late tertiary follicles and corpus lutea and a lower number of early tertiary follicles in the HFF/FW mice treated with anti-IL-10 mAb showed that antagonism of IL-10 activities appeared to reverse the pathohistological changes induced by the HFF/FW diet (Figure 7C). Again, this effect was not seen in the STD mice (Figure 7D).

3.8. A schematic of the proposed effect of the HFF/FW diet on follicular development

A schematic of our findings is presented in Figure 7E. In summary, our study demonstrated that the HFF/FW diet in the mice induced hypertrophy of the POATs, which caused an upregulation of IL-10. This upregulation of IL-10 may have disrupted normal folliculogenesis between the early and late tertiary follicle stages, possibly from defective angiogenesis mediated by IL-10, which antagonized VEGF-activated pathways such as NF-κB and PI3K/AKT.

4. DISCUSSION

Although not a cardinal manifestation of PCOS, obesity nonetheless occurs at higher frequency in patients with PCOS and has exhibited modulating effects on its clinical manifestation [4]. A modulating effect by obesity on the manifestation of menstrual regularity is of particular clinical interest, as it represents one of the cardinal symptoms of PCOS [2]. This relationship is of academic interest as it appears to bridge two distinct functional systems—the metabolic and reproductive systems. Prior studies have generally focused on the cross-reactivity of insulin on the steroid pathways [26,27] and conversely the metabolic effects of hyperandrogenism [28]. However, some studies have noted that the occurrence of ovulatory dysfunctions may be independent of insulin resistance [4], which hinted at alternative pathways.

In this study, we present a potential pathway linking obesity to derangements in follicular development. Obesity was induced in female mice using an obesogenic diet consisting of high-fat feed and fructose water. Histopathology and IHC showed attenuation of follicular developments in the context of decreased microvessel counts in the early follicles. Adipokine screen of the POATs showed a progressive increase in IL-10 expression that occurred with the increased duration of the HFF/FW diet. Experimentally, IL-10 was shown to disrupt the VEGF-induced angiogenesis in an endothelial cell model. Mitigation of this altered folliculogenesis was seen following the in vivo administration of anti-IL-10 mAb in the HFF/FW mice.

Based on the results of this study, we assert that obesity induces a rise in IL-10, which causes a disruption in follicular development via defective vascular formation. Disrupted vascular proliferation, migration, and permeability by IL-10 in the angiogenesis model support this assertion. Furthermore, we were able to identify a cell-level effect, whereby IL-10 disrupted the NF-κB signaling and p-AKT expression that were inducible by VEGF. This is consistent with previous findings of IL-10 antagonism in VEGF-induced proliferations in models of tissue repair and neoplasm [29,30]. The disruptive role of IL-10 in folliculogenesis is also highly suspected, as higher levels of IL-10 have been demonstrated in the serum [31], visceral fats [32], and follicular fluids [33,34] of obese individuals and in the follicular fluids of patients with PCOS [35]. However, no study has to date linked IL-10 to impaired folliculogenesis via disrupted VEGF signaling.

VEGF has been shown to be an important regulator in the formation and selection of follicles in mammals. VEGF-mediated angiogenesis regulates the follicular supply of gonadotropins, growth factors, oxygen, and steroid precursors, which determines follicular growth [36]. Direct VEGF injections have increased the vascular density of follicles and number of mature follicles [37,38], while VEGF antagonists have induced arrest of angiogenesis and antrum formation [39]. Given the role of VEGF in folliculogenesis and the disruptive effects of IL-10 on VEGF-dependent angiogenesis, the increased production of IL-10 in the HFF/FW mice could explain the lower number of microvessels in the early tertiary follicles. This may in turn decrease the number of late tertiary follicles and corpus lutea via decreased blood supply, which restricts growth [36]. The observed window of follicular disruption between early and late tertiary follicles also coincides with the reported period of increased VEGF expression [40]. As mitigation of these adverse findings followed the administration of neutralizing IL-10 antibodies, the culpability of IL-10 was further strengthened.

Other secretomes of adipose origin have previously been shown to increase with obesity, including an exhaustive list of leptin, adiponectin, tumor necrosis factor alpha (TNFα), resistin, IL-6, IL-18, lipocalin 2, monocyte chemoattractant protein (MCP-1), RBP4, SFRP5,
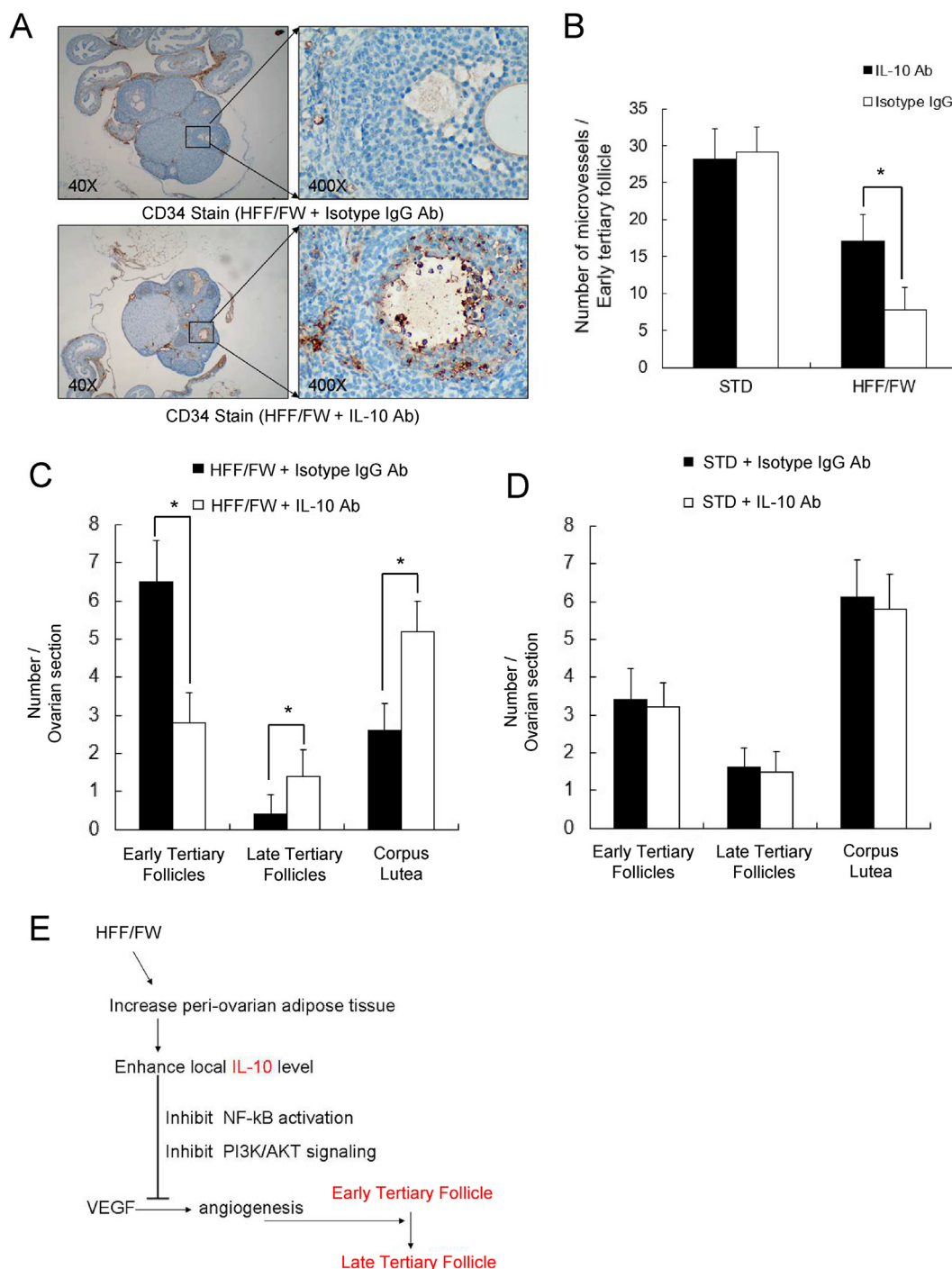
Figure 7: Anti-IL-10 mAb prevented changes in ovarian follicular angiogenesis and follicular maturity induced by HFF/FW *in vivo*. Mice were treated with anti-IL-10 mAb (intraperitoneal, 100 μg/mouse, twice weekly) and isotype IgG under conditions of HFF/FW and STD. (A) CD34 staining in the anti-IL-10 mAb-treated HFF/FW mice showed increased numbers of microvessels. (B) Quantification of microvessel counts showed a significant increase in microvessel counts with the administration of anti-IL-10 mAb in the HFF/FW mice. (C) Quantified early and late tertiary follicles (Graafian follicles) and corpus lutea counts showed significantly decreased early tertiary follicles and increased late tertiary follicles and corpus lutea following anti-IL-10 mAb in the HFF/FW mice. (D) The early and late tertiary follicles and corpus lutea counts were not significantly different following anti-IL-10 mAb in the STD mice. (E) A schematic of the possible effects of the HFF/FW diet on the regulation of early to late tertiary follicle development. Quantified results are expressed as mean ± SD; (*) marks statistically significant differences between groups ($P < 0.05$); N = 10 for all the groups.

ANGPTL2, CXCL5, and visfatin [41—43]. With the exception of IL-18, SFRP5, CXCL5, and visfatin, the majority of the listed adipokines was included in the initial adipokine screen utilized in this study. Of the well-documented pro-inflammatory molecules, leptin, resistin, and IL-6 all exhibited increases in response to obesity, consistent with the

literature [41—43]. However, there were temporal variations in their increases, with leptin showing an early rise at 2 weeks, and resistin and IL-6 at 4 weeks (Figure 3A and Supplementary Table 1). We did not detect an increase in TNFα or MCP-1, although this could have been due to the shorter duration of the current study. A recent study

posited that the origin of TNFα in adipose may be exclusively macrophages [44]. In combination with the finding that obesity-induced macrophage infiltration of the adipose is a late-occurring event that only becomes detectable after 16 weeks of a high-fat diet [45], this could explain the low number of macrophages and low levels of TNFα and MCP-1 in this study. In contrast, IL-10 has been shown to be predominantly produced by adipocytes in human [32,46], murine [32], and various adipocyte cell lines of human [47] and murine [48] origin. This could be why there were immediate and progressive increases in IL-10 and why the IL-10-specific stains localized around the adipocytes in this study.

The limitations of this study are as follows. Although we initially identified the increased IL-10 from the POATs, whether this was the main source of IL-10 acting on the ovaries is unknown. However, the biological likelihood of a POAT origin is high, given that the visceral adipose is a known producer of IL-10 in obesity [32], and IL-10 is a molecule of autocrine and paracrine control, rather than endocrine [49]. The POATs are known to have paracrine control over the ovaries [19], and the mesothelium appears permissive to the transit of soluble molecules larger than IL-10 [50]. We also noted higher concentrations of IL-10 in the POATs than the serum. Regardless of the source, IL-10 concentrations should be supraphysiological in the ovarian compartments of the obese, as this has been repeatedly demonstrated in follicular fluids [33,34] and visceral fat depots [32,51]. Second, although the POATs are considered functionally analogous to the visceral fats of humans [52], there are no strict anatomical counterparts. Third, although we proposed a possible mechanism linking obesity and disrupted folliculogenesis, this may not be the only regulatory factor involved in menstrual regularity. Finally, the duration of this study was short, which limited our ability to predict long-term reproductive derangements. We do not know whether these histopathological alterations definitively cause reproductive deficiencies.

In conclusion, we present a possible pathway linking obesity and disrupted folliculogenesis that is mediated by the increased production of IL-10 in the visceral fats. The findings of this study may help clarify the cause of obesity-associated ovulatory dysfunction in PCOS and provide future targets for therapeutic interventions. However, more work is needed to validate these findings in humans.

FINANCIAL SUPPORT

DATA AVAILABILITY STATEMENT

The data will be made available on reasonable request.

AUTHOR ROLES

Po-Kai Yang: Writing original draft, visualization, formal analysis, software, investigation, and validation. **Chia-Hung Chou:** Investigation, visualization, data curation, conceptualization, and methodology. **Chu-Chun Huang:** Conceptualization and resources. **Shin-Fu Chen:** Writing, review, and editing. **Wen-Fen Wen:** Resources and validation. **Chia-Tung Shun:** Resources and validation. **Hong-Nerng Ho:** Supervision, writing, review, and editing. **Mei-Jou Chen:** Funding acquisition, project administration, and visualization.

CONFLICT OF INTEREST

None.

ACKNOWLEDGMENTS

APPENDIX A. SUPPLEMENTARY DATA

Supplementary data to this article can be found online at https://doi.org/10.1016/j.molmet.2021.101189.

REFERENCES

[1] Zawadzki, J.K., Dunaif, A., 1992. Diagnostic criteria for polycystic ovary syndrome: towards a rational approach. Polycystic ovary syndrome, 377—384.

[2] Rotterdam Consensus Workshop Group, 2004. Revised 2003 consensus on diagnostic criteria and long-term health risks related to polycystic ovary syndrome. Fertility and Sterility 81(1):19—25.

[3] Azziz, R., Woods, K.S., Reyna, R., Key, T.J., Knochenhauer, E.S., Yildiz, B.O., 2004. The prevalence and features of the polycystic ovary syndrome in an unselected population. Journal of Clinical Endocrinology & Metabolism 89(6): 2745—2749.

[4] Rojas, J., Chávez, M., Olivar, L., Rojas, M., Morillo, J., Mejías, J., et al., 2014. Polycystic ovary syndrome, insulin resistance, and obesity: navigating the pathophysiologic labyrinth. International Journal of Reproductive Medicine 2014:719050.

[5] Chen, M.-J., Yang, W.-S., Chen, C.-L., Wu, M.-Y., Yang, Y.-S., Ho, H.-N., 2008. The relationship between anti-Müllerian hormone, androgen and insulin resistance on the number of antral follicles in women with polycystic ovary syndrome. Human Reproduction 23(4):952—957.

[6] Moran, C., Tena, G., Moran, S., Ruiz, P., Reyna, R., Duque, X., 2010. Prevalence of polycystic ovary syndrome and related disorders in Mexican women. Gynecologic and Obstetric Investigation 69(4):274—280.

[7] Franks, S., Stark, J., Hardy, K., 2008. Follicle dynamics and anovulation in polycystic ovary syndrome. Human Reproduction Update 14(4):367—378.

[8] Patel, R., Shah, G., 2018. High-fat diet exposure from pre-pubertal age induces polycystic ovary syndrome (PCOS) in rats. Reproduction (Cambridge, England) 155(2):141—151.

[9] Nteeba, J., Ganesan, S., Keating, A.F., 2014. Progressive obesity alters ovarian folliculogenesis with impacts on pro-inflammatory and steroidogenic signaling in female Mice1. Biology of Reproduction 91(4):86.

[10] Newell-Fugate, A.E., Taibl, J.N., Alloosh, M., Sturek, M., Bahr, J.M., Nowak, R.A., et al., 2015. Effects of obesity and metabolic syndrome on steroidogenesis and folliculogenesis in the female Ossabaw mini-pig. PloS One 10(6):e0128749.

[11] Norman, R.J., Noakes, M., Wu, R., Davies, M.J., Moran, L., Wang, J.X., 2004. Improving reproductive performance in overweight/obese women with effective weight management. Human Reproduction Update 10(3):267—280.

[12] Moran, L.J., Brinkworth, G.D., Norman, R.J., 2008. Dietary therapy in polycystic ovary syndrome. Seminars in Reproductive Medicine 26(1):85—92.

[13] Bohler, H., Mokshagundam, S., Winters, S.J., 2010. Adipose tissue and reproduction in women. Fertility and Sterility 94(3):795—825.

[14] Escobar-Morreale, H.F., San Millán, J.L., 2007. Abdominal adiposity and the polycystic ovary syndrome. Trends in Endocrinology and Metabolism 18(7): 266—272.

[15] Barber, T.M., Franks, S., 2013. Adipocyte biology in polycystic ovary syndrome. Molecular and Cellular Endocrinology 373(1—2):68—76.

Original Article

[16] Van Der Lee, S., Boot, L.M., 1955. Spontaneous pseudopregnancy in mice. Acta Physiologica et Pharmacologica Neerlandica 4(3):442—444.

[17] Whitten, W.K., 1956. Modification of the oestrous cycle of the mouse by external stimuli associated with the male. Journal of Endocrinology 13(4): 399—404.

[18] Goldman, K.N., Chenette, D., Arju, R., Duncan, F.E., Keefe, D.L., Grifo, J.A., et al., 2017. mTORC1/2 inhibition preserves ovarian function and fertility during genotoxic chemotherapy. Proceedings of the National Academy of Sciences of the U S A 114(12):3186—3191.

[19] Yang, L., Chen, L., Lu, X., Tan, A., Chen, Y., Li, Y., et al., 2018. Peri-ovarian adipose tissue contributes to intraovarian control during folliculogenesis in mice. Reproduction (Cambridge, England) 156(2):133—144.

[20] Xiao, S., Duncan, F.E., Bai, L., Nguyen, C.T., Shea, L.D., Woodruff, T.K., 2015. Size-specific follicle selection improves mouse oocyte reproductive outcomes. Reproduction (Cambridge, England) 150(3):183—192.

[21] Chen, M.-J., Peng, Y., Yang, Y.-S., Huang, S.-C., Chow, S.-N., Torng, P.-L., 2005. Increased hyaluronan and CD44 expressions in intravenous leiomyomatosis. Acta Obstetricia et Gynecologica Scandinavica 84(4):322—328.

[22] Ballak, D.B., Stienstra, R., Hijmans, A., Joosten, L.A., Netea, M.G., Tack, C.J., 2013. Combined B- and T-cell deficiency does not protect against obesity-induced glucose intolerance and inflammation. Cytokine 62(1):96—103.

[23] Abràmoff, M.D., Magalhães, P.J., Ram, S.J.J.B.i., 2004. Image processing with ImageJ 11(7):36—42.

[24] Pourgholami, M.H., Khachigian, L.M., Fahmy, R.G., Badar, S., Wang, L., Chu, S.W.L., et al., 2010. Albendazole inhibits endothelial cell migration, tube formation, vasopermeability, VEGF receptor-2 expression and suppresses retinal neovascularization in ROP model of angiogenesis. Biochemical and Biophysical Research Communications 397(4):729—734.

[25] Geva, E., Jaffe, R.B., 2000. Role of vascular endothelial growth factor in ovarian physiology and pathology. Fertility and Sterility 74(3):429—438.

[26] Willis, D., Franks, S., 1995. Insulin action in human granulosa cells from normal and polycystic ovaries is mediated by the insulin receptor and not the type-I insulin-like growth factor receptor. Journal of Clinical Endocrinology & Metabolism 80(12):3788—3790.

[27] Brothers, K.J., Wu, S., DiVall, S.A., Messmer, M.R., Kahn, C.R., Miller, R.S., et al., 2010. Rescue of obesity-induced infertility in female mice due to a pituitary-specific knockout of the insulin receptor. Cell Metabolism 12(3): 295—305.

[28] Barber, T.M., Hanson, P., Weickert, M.O., Franks, S., 2019. Obesity and polycystic ovary syndrome: implications for pathogenesis and novel management strategies. Clinical Medicine Insights: Reproductive Health 13, 1179558119874042.

[29] Silvestre, J.S., Mallat, Z., Duriez, M., Tamarat, R., Bureau, M.F., Scherman, D., et al., 2000. Antiangiogenic effect of interleukin-10 in ischemia-induced angiogenesis in mice hindlimb. Circulation Research 87(6):448—452.

[30] Kohno, T., Mizukami, H., Suzuki, M., Saga, Y., Takei, Y., Shimpo, M., et al., 2003. Interleukin-10-mediated inhibition of angiogenesis and tumor growth in mice bearing VEGF-producing ovarian cancer. Cancer Research 63(16):5091—5094.

[31] Calcaterra, V., De Amici, M., Klersy, C., Torre, C., Brizzi, V., Scaglia, F., et al., 2009. Adiponectin, IL-10 and metabolic syndrome in obese children and adolescents. Acta BioMedica 80(2):117—123.

[32] Juge-Aubry, C.E., Somm, E., Pernin, A., Alizadeh, N., Giusti, V., Dayer, J.-M., et al., 2005. Adipose tissue is a regulated source of interleukin-10. Cytokine 29(6):270—274.

[33] La Vignera, S., Condorelli, R., Bellanca, S., La Rosa, B., Mousaví, A., Busà, B., et al., 2011. Obesity is associated with a higher level of pro-inflammatory cytokines in follicular fluid of women undergoing medically assisted procreation (PMA) programs. European Review for Medical and Pharmacological Sciences 15(3):267—273.

[34] Gonzalez, M.B., Lane, M., Knight, E.J., Robker, R.L., 2018. Inflammatory markers in human follicular fluid correlate with lipid levels and Body Mass Index. Journal of Reproductive Immunology 130:25—29.

[35] Zhang, T., Tian, F., Huo, R., Tang, A., Zeng, Y., Duan, Y.G., 2017. Detection of dendritic cells and related cytokines in follicular fluid of patients with polycystic ovary syndrome. American Journal of Reproductive Immunology 78(3).

[36] Kaczmarek, M.M., Schams, D., Ziecik, A.J., 2005. Role of vascular endothelial growth factor in ovarian physiology - an overview. Reproductive Biology 5(2): 111—136.

[37] Iijima, K., Jiang, J.Y., Shimizu, T., Sasada, H., Sato, E., 2005. Acceleration of follicular development by administration of vascular endothelial growth factor in cycling female rats. Journal of Reproduction and Development 51(1):161—168.

[38] Shimizu, T., Jiang, J.Y., Iijima, K., Miyabayashi, K., Ogawa, Y., Sasada, H., et al., 2003. Induction of follicular development by direct single injection of vascular endothelial growth factor gene fragments into the ovary of miniature gilts. Biology of Reproduction 69(4):1388—1393.

[39] Zimmermann, R.C., Hartman, T., Kavic, S., Pauli, S.A., Bohlen, P., Sauer, M.V., et al., 2003. Vascular endothelial growth factor receptor 2-mediated angiogenesis is essential for gonadotropin-dependent follicle development. Journal of Clinical Investigation 112(5):659—669.

[40] Yamamoto, S., Konishi, I., Tsuruta, Y., Nanbu, K., Mandai, M., Kuroda, H., et al., 1997. Expression of vascular endothelial growth factor (VEGF) during folliculogenesis and corpus luteum formation in the human ovary. Gynecological Endocrinology 11(6):371—381.

[41] Ouchi, N., Parker, J.L., Lugus, J.J., Walsh, K., 2011. Adipokines in inflammation and metabolic disease. Nature Reviews Immunology 11(2):85—97.

[42] Cao, H., 2014. Adipocytokines in obesity and metabolic disease. Journal of Endocrinology 220(2):T47—T59.

[43] Song, J., Deng, T., 2020. The adipocyte and adaptive immunity. Frontiers in Immunology 11:593058.

[44] Ebke, L.A., Nestor-Kalinoski, A.L., Slotterbeck, B.D., Al-Dieri, A.G., Ghosh-Lester, S., Russo, L., et al., 2014. Tight association between macrophages and adipocytes in obesity: implications for adipocyte preparation. Obesity 22(5): 1246—1255.

[45] Xu, H., Barnes, G.T., Yang, Q., Tan, G., Yang, D., Chou, C.J., et al., 2003. Chronic inflammation in fat plays a crucial role in the development of obesity-related insulin resistance. Journal of Clinical Investigation 112(12):1821—1830.

[46] Skurk, T., Alberti-Huber, C., Herder, C., Hauner, H., 2007. Relationship between adipocyte size and adipokine expression and secretion. Journal of Clinical Endocrinology & Metabolism 92(3):1023—1033.

[47] Meijer, K., de Vries, M., Al-Lahham, S., Bruinenberg, M., Weening, D., Dijkstra, M., et al., 2011. Human primary adipocytes exhibit immune cell function: adipocytes prime inflammation independent of macrophages. PloS One 6(3):e17154.

[48] Bradley, R.L., Fisher, F.F., Maratos-Flier, E., 2008. Dietary fatty acids differentially regulate production of TNF-alpha and IL-10 by murine 3T3-L1 adipocytes. Obesity 16(5):938—944.

[49] Iyer, S.S., Cheng, G., 2012. Role of interleukin 10 transcriptional regulation in inflammation and autoimmune disease. Critical Reviews in Immunology 32(1): 23—63.

[50] Cotran, R.S., Karnovsky, M.J., 1968. Ultrastructural studies on the permeability of the mesothelium to horseradish peroxidase. The Journal of Cell Biology 37(1):123—137.

[51] Masi, L.N., Crisma, A.R., Martins, A.R., do Amaral, C.L., Torres, R.P., Mancini Filho, J., et al., 2016. Inflammatory state of periaortic adipose tissue in mice under obesogenic dietary regimens. Journal of Nutrition & Intermediary Metabolism 6:1—7.

[52] Chusyd, D.E., Wang, D., Huffman, D.M., Nagy, T.R., 2016. Relationships between rodent white adipose fat pads and human white adipose fat depots. Frontiers in Nutrition 3:10.